Supplementary Information

Porous Graphite Plate Design in SiC PVT Growth: Optimized Powder Source Evolution for Enhanced Crystal Yield and Quality

*Yang Chen, [a] Xiaofang Ye, [a] Shilin Liu, [a] Wenyu Kang, *[a] Wei Jiang, [a] Jun Yin, *[a] and Junyong Kang [a]*

Pen-Tung Sah Institute of Micro-Nano Science and Technology, Engineering Research Center of Micro-Nano Optoelectronic Materials and Devices, MOE, College of Physical Science and Technology, Tan Kah Kee Innovation Laboratory (FDIX), Xiamen University, Xiamen 361005, China.

Email: wykang@xmu.edu.cn, jyin@xmu.edu.cn

1. Theoretical simulation model

The multi-physics model in this study coupled conjugate heat transfer, surface radiation, laminar flow, low-concentration species transport in porous media, and solid mechanics to construct a full-process simulation model. Experimental validation guided parameter calibration, requiring adjustment of the resistive heater power to maintain a seed surface temperature of 2200°C under an argon pressure of 5 torr. The SiC powder source material (particle diameter of 1 mm with

porosity of 0.65) were modelled as distinct porous media domains. The key material properties and parameters for simulation are summarized in **Table S1**.

Table S1. Material properties and parameters for simulation

Parameter	Value	significance
k_{crystal}	$451700\times T^{-1.29}$ (W m^{-1} K^{-1})	Thermal conductivity of crystal
$k_{\text{insulation}}$	$2.16\times10^{-9}\times T^{2}-1.43\times10^{-5}\times T+0.367$ (W m^{-1} K^{-1})	Thermal conductivity of insulation
k_{graphite}	$125868\ (T+165.9)^{-1}$ (W m^{-1} K^{-1})	Thermal conductivity of graphite
$\varepsilon_{\text{crystal}}$	0.9	Surface emissivity of crystal
$\varepsilon_{\text{insulation}}$	0.8	Surface emissivity of insulation
$\varepsilon_{\text{graphite}}$	0.8	Surface emissivity of graphite
ρ_{crystal}	1610 (kg m^{-3})	Density of crystal
$\rho_{\text{insulation}}$	160 (kg m^{-3})	Density of insulation
ρ_{graphite}	1850 (kg m^{-3})	Density of graphite
M_{crystal}	40 (g mol^{-1})	Molar mass of crystal
M_{graphite}	12 (g mol^{-1})	Molar mass of graphite
M_{SiC_2}	52 (g mol^{-1})	Molar mass of SiC_2
$\alpha_{SiC2}^{s/d}$	0.012	Adhesion coefficient of SiC_2
α	0.8	Correction coefficient of ΔA
v_{crystal}	0.3	Poisson's ratio of crystal
E_{crystal}	430 (GPa)	Young's modulus of crystal
α_{crystal}	4.5×10^{-6} (1/K)	Coefficient of thermal expansion of crystal
b_{crystal}	3.8×10^{-10} (m)	Burgers Vector of crystal

The coupled heat transfer model consisted of three primary mechanisms, including the conjugate heat conduction across solid-fluid interfaces, the thermal convection within the fluid phase, and the radiative heat transfer between solid surfaces. The temperature field was according to the energy conservation equation:[1, 2]

$$\rho C_p \frac{\partial T}{\partial t} + \nabla \cdot (-k\nabla T) = Q - \rho C_p u \cdot \nabla T + \varepsilon\sigma\left(T_\sigma^4 - T_\infty^4\right)\frac{\delta A}{\delta V} \tag{1}$$

where ρ is the material density, C_p is the specific heat capacity, k is the thermal conductivity coefficient, Q is the energy from the resistive heater, u is the fluid flow velocity, ε is the emissivity of solid surfaces, σ is the Stefan-Boltzmann constant, T_σ is the solid surface temperature, T_∞ is the fluid ambient temperature, and $\frac{\delta A}{\delta V}$ is the surface-to-volume differential ratio for radiation.

During the PVT growth of SiC crystals, the source material underwent sublimation and decomposition under resistive heating, producing vapor-phase species such as Si, SiC_2, and Si_2C.[3, 4] These species would diffuse along the temperature gradient within a low-pressure inert gas atmosphere, driven by concentration gradients. Supersaturation conditions would emerge at the seed crystal surface when the local vapor partial pressure surpassed the equilibrium vapor pressure at the given temperature, enabling epitaxial deposition of SiC. Based on the Hertz-Knudsen equation,[5] the net mass flux (*J*) of SiC sublimation and deposition per unit time were given by:

$$J_i^s = \alpha_i^s \frac{P_i^* - P_i}{\sqrt{2\pi M_i RT}} \tag{2}$$

$$J_i^d = \alpha_i^d \frac{P_i - P_i^*}{\sqrt{2\pi M_i RT}} \tag{3}$$

where J_i^s and J_i^d denote the molar flux of the *i*-th vapor component during sublimation at the source material surface and deposition at the seed crystal surface, respectively. α_i^s and α_i^d represent the

surface accommodation coefficients for sublimation and deposition of the *i*-th component. Specifically, the surface accommodation coefficients, which represent the kinetic sticking probabilities of vapor species, were referenced to quantitative values derived from *ab*-initio calculations by Alao *et al*.[6] These theoretical values were applied to accurately reflect the kinetic adsorption barriers governing the sublimation and deposition rates. P^*_i is the equilibrium vapor pressure of the *i*-th component at temperature *T* ($P^*_i(T) = Ae^{-E_a/RT}$).[7] P_i is the actual partial pressure of the *i*-th component. M_i is the molar mass, R is the ideal gas constant, and *T* is the temperature calculated from the heat transfer model.

To analyze reactions in the source chamber, the SiC decomposition was initiated at 2200°C when the equilibrium vapor pressure surpassed the local partial pressure, as dictated by the Hertz-Knudsen equation. This process produced vapor species including Si, SiC_2, and Si_2C. Non-stoichiometric decomposition preferentially released Si and would result in a carbon-enriched graphitization of the source material.[8] Simultaneously, convective flows drive recrystallization in the upper region of the source. To model these phenomena, a source evolution framework with two key assumptions was adopted: SiC source particles were spherical (1 mm in diameter) and retained their size during reaction. The reaction kinetics followed a volume-normalized rate equation:

$$R_i = J_i^s \frac{\Delta A}{\Delta V} \tag{4}$$

where R_i represents the reaction rate, J_i^s denotes the molar flux of source surface sublimation, and $\frac{\Delta A}{\Delta V}$ denotes specific surface area (SSA, which is quantified by the reaction intensity normalized by unit volume). In the formulation, the reaction rate is expressed as the product of the species flux and the reactive surface area. The activation energy for sublimation is implicitly embedded in the

temperature-dependent equilibrium vapor pressure term $P_i^*(T)$ within the Hertz-Knudsen equation (Eq. 2), which imparts an exponential dependence of the reaction potential on temperature. As a surface-mediated reaction, the reaction rate increased proportionally with the relative expansion of reactive surface area to volume. The parameter ΔA in the equation was defined as follows:

$$\Delta A = \alpha N_T A_c \tag{5}$$

where α denotes the correction coefficient, which was calibrated to be 0.8 in this study. This value was determined by fitting the simulated graphitization degree to the experimental C/Si atomic ratio. A_c represents the constant surface area of an individual particle, and N_T defines the particle count per unit volume, which could be expressed as:

$$N_T = \frac{\Delta V(1-\varepsilon)}{\frac{4}{3}\pi r^3} \tag{6}$$

where ΔV denotes the unit volume, ε represents the spatial porosity distribution within the powder source, r is the particle radius, and the volume ratio of SiC and C are derived from mass conservation governed by a constant-coefficient ordinary differential equation (ODE), formulated as:

$$\frac{\partial \gamma_{SiC}}{\partial t} = -\frac{M_{SiC} R_{SiC}}{\rho_{SiC}} \tag{7}$$

$$\frac{\partial \gamma_C}{\partial t} = \frac{M_C R_C}{\rho_C} \tag{8}$$

where γ_i represents the volume ratio of component i, M_i is its molar mass, R_i is the reaction rate, and ρ_i is bulk density. At the reaction temperature (from 2200 to 2500°C), the partial pressure ratio of vapor species is experimentally determined as $P_{Si} : P_{Si_2C} : P_{SiC_2} = 4 : 1 : 2$,[9] Given that Si vapor

pressure peaks at 2500°C and the stoichiometric Si:C ratio (1:1) must be conserved, the partial pressure of SiC_2 governs the growth rate of SiC single crystals,[10] leading to the relationship:

$$R_{SiC} = 2R_{SiC2} \tag{9}$$

$$R_C = 0.75R_{SiC2} \tag{10}$$

The established mathematical framework enabled time-dependent simulation of crystalline growth through the evolution of SiC and carbon volume ratio in the source chamber were calculated. This computation cascade thereby enabled the subsequent derivation of critical distributions: porosity (ε), thermal conductivity (k), bulk density (ρ), and heat capacity (C_p). The evolution of these thermophysical properties with growth time dynamically altered the thermal and flow fields within the crucible, ultimately governing the dynamic evolution of the crystallization interface.

The coupled mass transfer model within the growth chamber was established under two fundamental assumptions. Firstly, the fluid followed Newtonian incompressible behavior. Secondly, the buoyancy-driven natural convection was predominated, allowing the neglect of Stefan flow induced by sublimation gradients.[11] The governing equations, derived from the Navier-Stokes framework,[12, 13] included the momentum conservation equation:

$$\rho\frac{\partial\vec{u}}{\partial t} + \rho(\vec{u}\cdot\nabla)\vec{u} = -\nabla P + \mu\nabla^2\vec{u} + \rho g \tag{11}$$

$$\nabla\cdot(\rho\vec{u}) = 0 \tag{12}$$

where ρ is the density of the fluid phase, $\vec{u}$ is the velocity vector distribution of the fluid, P is the external pressure, μ is the dynamic viscosity coefficient, and g is the gravitational acceleration. The molar concentration of vapor-phase components was calculated using the convection-diffusion equation in the dilute species transport of porous media, expressed as:

$$\frac{\partial c_i}{\partial t} + \nabla \cdot (c_i u) = D_i \nabla^2 c_i \tag{13}$$

where c_i represents the molar concentration of each vapor-phase component, u the velocity, and D_i the diffusion coefficient of each component as given by:

$$D_i = D_0 \frac{P_0}{P} \left(\frac{T}{T_0} \right)^n \tag{14}$$

where D_0 the binary diffusion coefficient between each vapor-phase component and the inert gas can be obtained through Graham's law of diffusion.[14] The argon gas with the crucible pressure controlled at 5 torr was used in this work. P_0 and T_0 are the reference pressure and temperature, are set as 1.013×10^5 Pa and 273 K, respectively. P and T represent the actual pressure and temperature at each time step, with the exponent n taken as 1.8.

The growth rate of the SiC single crystal at this reaction temperature was constrained by the rate-limiting species flux J_{SiC2}^{d} due to mass conservation, leading to the following expression for the SiC growth rate:

$$G_{SiC} = \frac{2M_{SiC}}{\rho_{SiC}} J_{SiC2} \tag{15}$$

where G_{SiC} is the growth rate of the SiC single crystal, M_{SiC} is the molar mass of SiC, and ρ_{SiC} is the material density. The numerical model implemented arbitrary Lagrangian-Eulerian (ALE) method in COMSOL with user-defined functions (UDFs) that dynamically updated the growth front position based on real-time G_{SiC} calculations. Adaptive remeshing was triggered at each time step to mitigate mesh distortion. This dual approach of ALE motion and adaptive remeshing ensured numerical stability and accuracy throughout the simulation.

Crystalline quality was critically influenced by thermoelastic effects during growth. Thermal gradients induce heterogeneous stress fields, where shear stress surpassing the critical threshold

triggers dislocation glide on basal planes, generating basal plane dislocations (BPDs).[15] These defects act as recombination centers and charge trapping sites, exacerbating gate oxide degradation in bipolar devices.[16] Minimizing BPD density is therefore paramount for device reliability. According to linear thermal stress theory, the components of the strain tensor were linear functions of the stress tensor, and the thermoelastic relationship was governed by Hooke's law as follows:

$$\sigma_{ij} = C_{ijkl}(\varepsilon_{kl} - \alpha(T - T_0)) \tag{16}$$

where σ_{ij} is the stress tensor, C_{ijkl} the anisotropic elastic stiffness tensor of the SiC crystal,[17] ε_{kl} the strain tensor, and α the temperature-dependent thermal expansion coefficient of SiC.[18] After obtaining the shear thermal stress in the SiC crystal, the dislocation density was calculated based on the difference between the shear stress and the critical shear stress, as given by:

$$N = \left[\frac{1 - v}{Gb}(\delta - \delta^{cr})\right]^2 \tag{17}$$

where N is the dislocation density, v is the Poisson's ratio of the SiC crystal, G is the shear modulus, b is the Burgers vector of dislocations, δ is the applied shear thermal stress at the point, and δ^{cr} is the critical shear stress. This study evaluated key SiC crystal growth metrics, including growth rate, surface morphology, thickness, dislocation density, and source utilization efficiency.

2. Supplementary figures

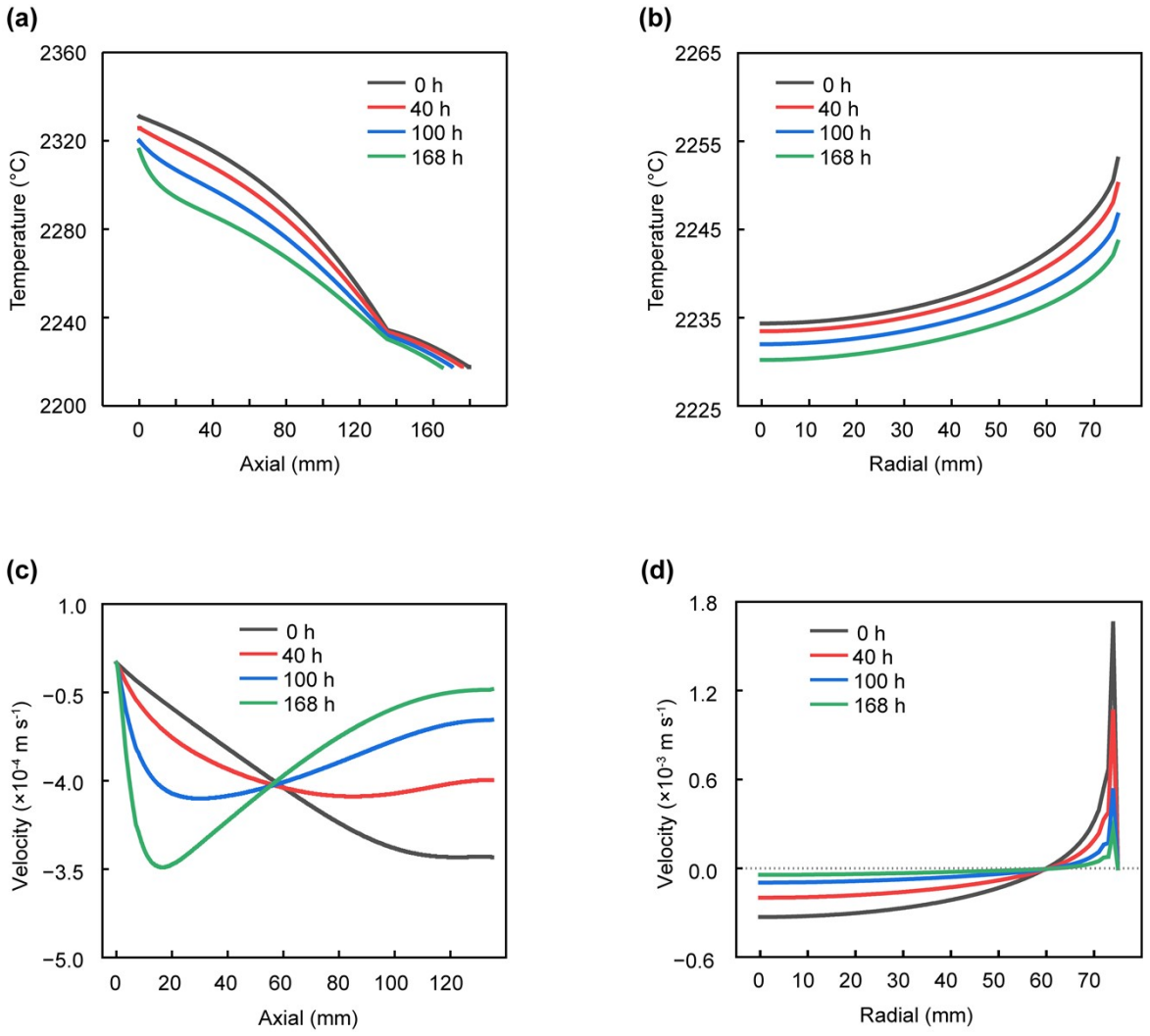

Figure S1. (a) Axial temperature profiles at crucible centerline (0 h, 40 h, 100 h, 168 h). (b) Radial temperature distributions on source surface at corresponding stages.(c) Axial velocity profiles along the source compartment centerline (0 h, 40 h, 100 h, 168 h), negative values indicate downward flow. (d) Radial velocity distributions on the source surface at corresponding stages.

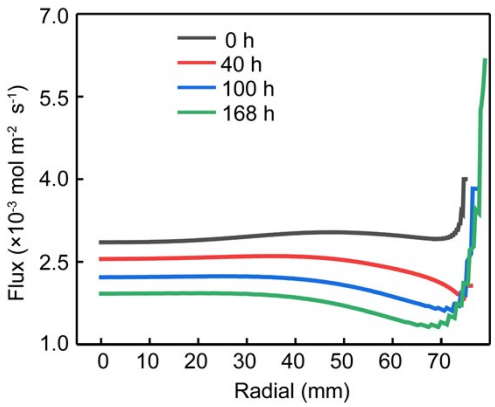

Figure S2. Radial flux distributions of dominant vapor species at the growth interface across time points.

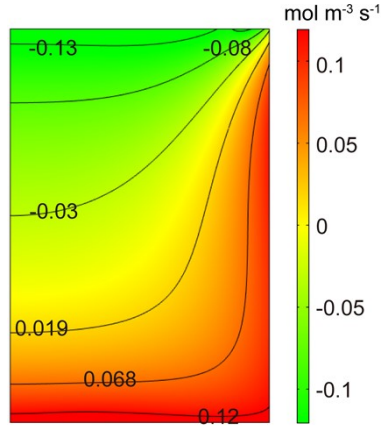

Figure S3. Distribution of SiC gasification rate in initial stage.

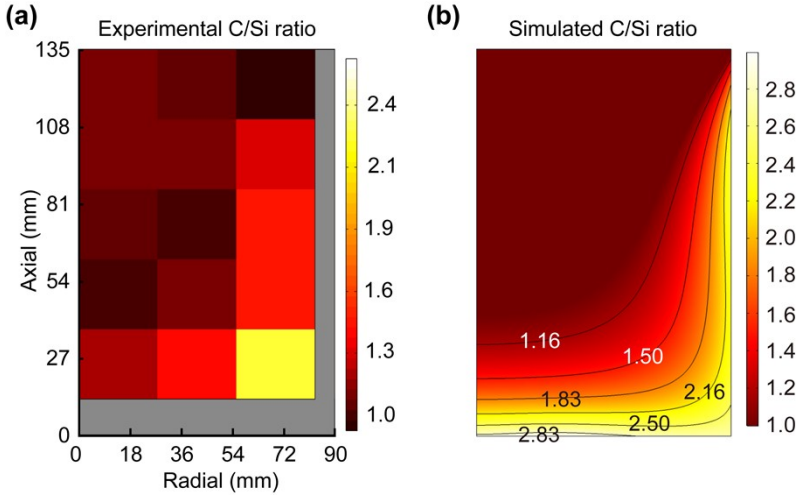

Figure S4. Comparative (a) XPS-measured versus (b) simulated C/Si atomic ratio profiles in post-growth source material (40 h).

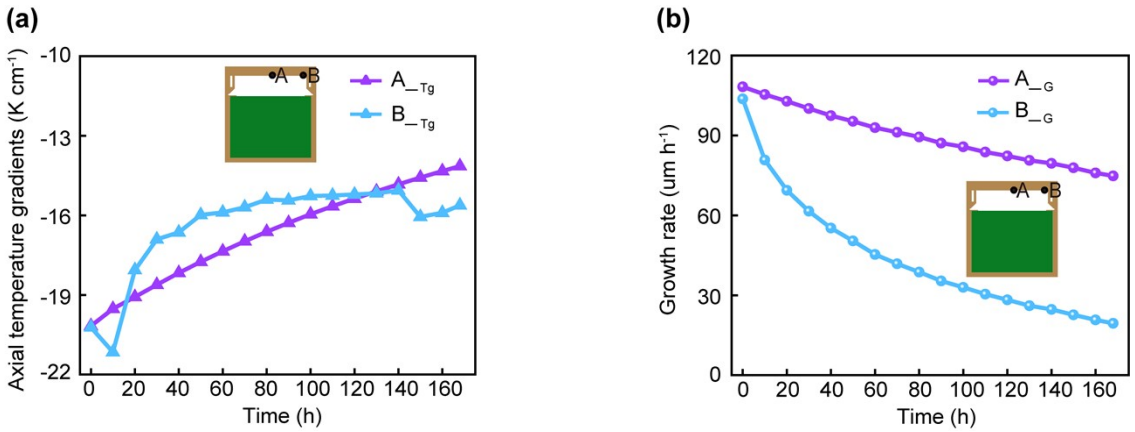

Figure S5. (a) Temporal evolution of axial temperature gradients at the center ($A_{\_Tg}$) and edge position ($B_{\_Tg}$). (b) Temporal evolution of growth rates at the center ($A_{\_G}$) and edge position ($B_{\_G}$).

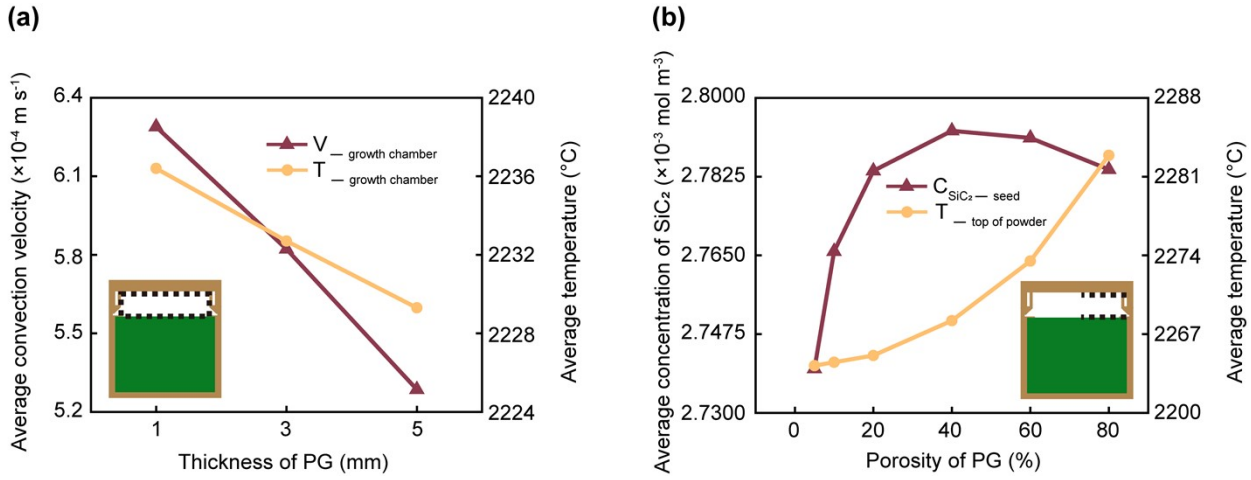

Figure S6. (a) Thickness dependent average convection velocity and average chamber temperature of the PG plate. (b) Porosity-dependent average temperature near the seed crystal and average SiC_2 concentration at the powder surface.

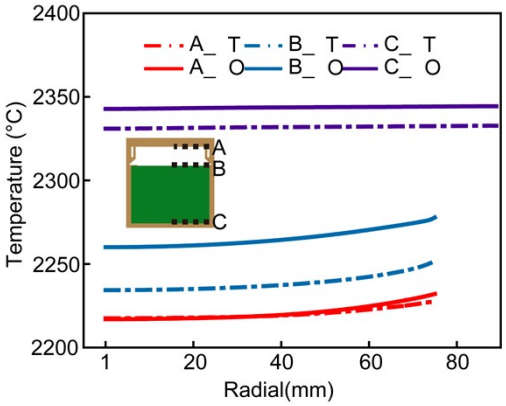

Figure S7. Radial temperature distributions at seed surface (A), source surface (B), and source base (C) between structures.

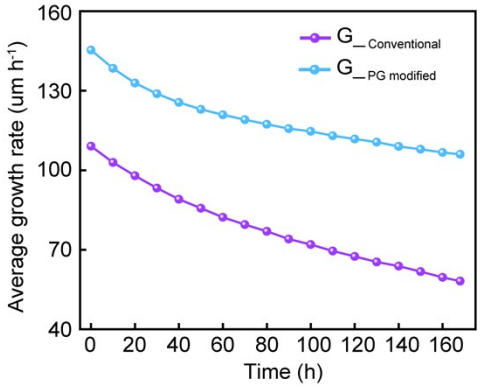

Figure S8. Temporal evolution of average growth rates in conventional structure($G_{\_Conventional}$) and PG design ($G_{\_PG}$).

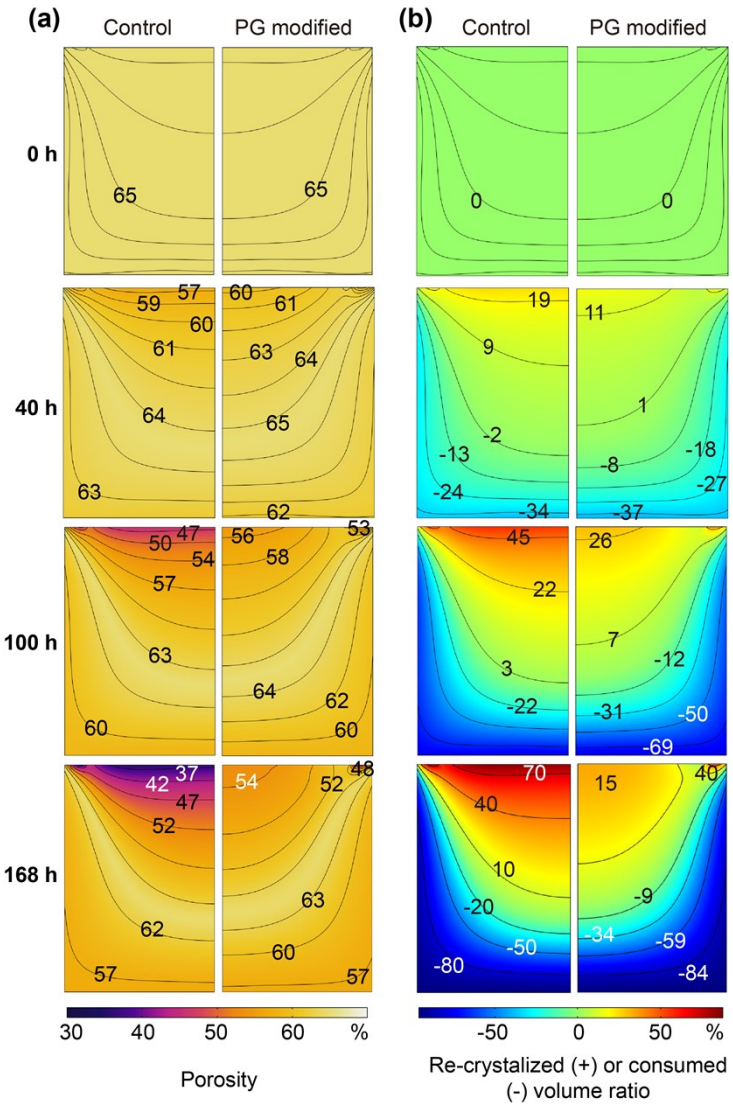

Figure S9. Spatiotemporal evolution of porosity and SiC volume ratio depletion in the source chamber for conventional and PG design structure (0 h, 40 h, 100 h and 168 h).

REFERENCES

1. Q.-S. Chen, H. Zhang, V. Prasad, C. Balkas and N. Yushin, *J. Heat Transfer*, 2001, **123**, 1098-1109.
2. H. Luo, X. Han, Y. Huang, D. Yang and X. Pi, *Crystals*, 2021, **11**, 1581.
3. H. Kleykamp and G. Schumacher, *Ber. Bunsenges. Phys. Chem.*, 1993, **97**, 799-804.
4. R. Olesinski and G. Abbaschian, *Bull. Alloy Phase Diagrams*, 1984, **5**, 486-489.
5. A. Segal, A. Vorob'ev, S. Y. Karpov, Y. N. Makarov, E. Mokhov, M. Ramm, M. Ramm, A. Roenkov, Y. A. Vodakov and A. Zhmakin, *Mater. Sci. Eng., B*, 1999, **61**, 40-43.

6. A. A. Alao, W.-N. Wu and W.-D. Hsu, *Vacuum*, 2022, **205**, 111414.
7. S. Lilov, *Mater. Sci. Eng., B*, 1993, **21**, 65-69.
8. S. Lilov, *Comput. Mater. Sci*, 1993, **1**, 363-368.
9. R.-H. Ma, H. Zhang, S. Ha and M. Skowronski, *J. Cryst. Growth*, 2003, **252**, 523-537.
10. Q.-S. Chen, J.-Y. Yan and V. Prasad, *J. Cryst. Growth*, 2007, **303**, 357-361.
11. W. D. Callister Jr and D. G. Rethwisch, *Materials Science and Engineering:An Introduction*, John wiley & sons, 2020.
12. G. K. Batchelor, *An Introduction to Fluid Dynamics*, Cambridge university press, 2000.
13. C. Depcik and S. Loya, *in Advanced Methods for Practical Applications in Fluid Mechanics*, intechOpen, 2012.
14. J. Dong, Z. Liu and X.-g. Xu, *J. Synth. Cryst.*, 2004, **33**, 283-287.
15. A. Jordan, R. Caruso, A. VonNeida and J. Nielsen, *J. Appl. Phys.*, 1981, **52**, 3331-3336.
16. H. Lendenmann, F. Dahlquist, N. Johansson, R. Söderholm, P. Nilsson, J. Bergman and P. Skytt, 2001, **353-356**,727-730.
17. Z. Li and R. C. Bradt, *Int. J. High Technol. Ceram.*, 1988, **4**, 1-10.
18. Z. Zhang, J. Lu, Q. Chen and V. Prasad, *Acta Mech. Sin*, 2006, **22**, 40-45.